Polymerization of Methyl Methacrylate in the Presence of a Nonpolar Hydrocarbon Solvent. I. Construction of a Complete Ternary Phase Diagram Through an *In Situ* Polymerization

Yunju Jung,[1] Carla Vanesa Luciani,[1,2] Joong Jin Han,[1] Kyu Yong Choi[1]

[1]*Department of Chemical and Biomolecular Engineering, University of Maryland, College Park, Maryland 20742*
[2]*INTEC (Universidad Nacional del Litoral—CONICET), Güemes 3450, Santa Fe S3000GLN, Argentina*

Received 21 October 2009; accepted 4 December 2009
DOI 10.1002/app.31924
Published online 22 February 2010 in Wiley InterScience (www.interscience.wiley.com).

ABSTRACT: This article presents the ternary phase diagram for methyl methacrylate (MMA), poly(methyl methacrylate) (PMMA), and *n*-hexane system at 70°C. It was constructed by both theoretical calculations and online laser light scattering (LLS) technique. *In situ* polymerization of MMA in a nonpolar nonsolvent carried out in a LLS cell provides a new means for the accurate detection of the cloud points of highly viscous polymer mixtures, with polymer weight fractions over 0.6. The ternary phase diagram measured in this study can be used to design the reaction conditions for the precipitation and/or dispersion polymerization in a nonpolar nonsolvent medium where polymerization kinetics as well as polymer particle morphologies are strongly affected by thermodynamic phase separation phenomena. © 2010 Wiley Periodicals, Inc. J Appl Polym Sci 116: 3648–3658, 2010

Key words: phase diagrams; light scattering; phase separation; poly(methyl methacrylate); dispersion polymerization

INTRODUCTION

The knowledge of multicomponent phase separation phenomena is crucial in many reactive polymerization systems. For instance, the synthesis of micron-sized polymer particles with complex internal morphologies such as hollows, multihollows, and multiporous structures is of growing recent interest in many technological applications such as microelectronic displays and microencapsulation. The direct synthesis of such materials is carried out in heterogeneous processes with controlled phase separation mechanisms. In such systems, detailed knowledge of heterogeneous polymerization kinetics and phase separation phenomena is essential for investigating the process characteristics. Varying the initial conditions for the phase separation in precipitation and dispersion polymerizations, final particles morphology may change from almost monodisperse polymer particles to complex porous polymeric structures. Also, the polymer molecular structure and final morphology of commercially important polymers such as poly(vinyl chloride), polyacrylonitrile, and high-impact polystyrene are strongly affected by the reaction-induced phase separation.[1–3] The knowledge of multicomponent phase separation phenomena is also crucial in many nonreactive systems. For instance, the final properties of asymmetric polymer membranes produced by the "wet inversion method" (i.e., immersion of a polymer solution in a coagulation bath) is determined by the thermodynamics and kinetics of the phase separation process.[4–9] In all of these heterogeneous processes, the system evolution depends on the composition and molecular characteristics of the coexisting phases and on the characteristics of the interface. The composition of the phases is usually determined by equilibrium conditions. For both the qualitative and quantitative understanding of heterogeneous processes, it is essential to have available an accurate phase diagram.

Many of the polymerization systems that undergo a phase separation process consist of two low molar mass liquid components (e.g., a solvent and a nonsolvent) and a polymer, and hence a ternary phase diagram is needed. Conventional methods to construct ternary phase diagrams of polymer/solvent/nonsolvent systems consist in either titrating polymer/solvent solutions or preparing a series of polymer/solvent/nonsolvent blends. In the titration method, transparent polymer/solvent solutions of known compositions are prepared, and the nonsolvent is slowly doled into the solutions until they

The first two authors contributed equally to this article.
Correspondence to: K. Y. Choi (choi@umd.edu).

turn turbid as polymer starts to precipitate.[3,6,8–12] This technique works very well for low polymer concentrations but it is hard to apply when the concentration of polymer is relatively high; the high viscosity of the polymer/solvent solution prohibits the uniform mixing of the added nonsolvent and generates the appearance of local turbidity.[3] As a result, it is difficult to accurately detect the exact cloud points. In the blending method, a set of polymer/solvent/nonsolvent mixtures of known compositions are prepared to determine which of them undergo a phase separation process.[5,7,13,14] Typically, the mixtures are first heated at a relatively high temperature until clear solutions are observed, and the samples are then cooled to a desired temperature. This technique requires the preparation of a vast number of samples to obtain a good representation of the ternary phase diagram, and it cannot be used when one of the species reacts at high temperatures (e.g., monomer).

One of the most challenging problems related to the techniques described above is the detection of the onset of turbidity (cloud point). Certainly, visual examination of the samples is the most widely used method.[3,5–13] Based on the huge difference of light scattered by a homogeneous solution with respect to that scattered by a precipitating mixture, an alternative method to determine the cloud points of a polymer solution is to use a light scattering technique. For example, methacrylic acid was polymerized in a light scattering cell in the presence of water and 2,2′-azobis(2-amidonopropane)-dihydrochloride as initiator.[15] Polymerizing samples were irradiated with a laser beam, and the scattered light at 0 degree angle was recorded. Cloud points containing 3 to 15 wt % of polymer were detected when a sharp decrease in the recorded intensity was observed. However, this technique was applied to determine cloud points close to the critical point of the methacrylic acid/polymethacrylic acid/water system, in a region containing over 80% of water.[15]

In this work, we used a laser light scattering (LLS) technique to determine the cloud points for the ternary system of methyl methacrylate (MMA), poly(-methyl methacrylate) (PMMA), and a nonpolar nonsolvent (for the polymer) such as *n*-hexane. Differently from the work by Aggarwal et al.[15], the *in situ* polymerization with LLS technique was applied to determining the "complete" ternary diagram, including the region of cloud points with very low concentration of monomer and nonsolvent. To this purpose, MMA was polymerized in a heated LLS cell in the presence of the nonsolvent and a peroxide initiator. The onset of turbidity was detected by recording the scattered light at a single angle. Visual examination method was also employed, though limited to cloud points of low PMMA concentrations, and the results were compared with those by the LLS technique. The experimental data were used to adjust the monomer-nonsolvent interaction parameter, and to compute the binodal curve, spinodal curve, and system tie lines using the Flory-Huggins (FH) theory. With the help of the theoretical results, some insights were drawn on the effects of the initial nonsolvent content on precipitation and/or dispersion polymerization of MMA in a nonpolar medium.

EXPERIMENTAL

Materials

MMA (Sigma-Aldrich), *n*-hexane (Fisher), and lauroyl peroxide (LPO) (Atochem) were used as monomer, nonsolvent, and initiator, respectively. Both the monomer and nonsolvent were purified by ion-exchange columns, while the initiator was used as received. PMMA standards of polydispersity below 1.09 and weight-average molecular weights of 625,500; 138,500; 60,150; 30,530; 10,290; and 3,810 g/mol were purchased from Polymer Laboratories. Methacryloxypropyl-terminated polydimethylsiloxane (PDMS) of molecular weight between 4000 and 6000 g/mol was purchased from Gelest.

Determination of cloud points by *in situ* polymerization

In this work, cloud points for the PMMA/MMA/*n*-hexane system were determined by conducting *in situ* polymerization experiments of MMA in the presence of *n*-hexane. The proposed technique aims at overcoming the drawbacks of the conventional titration method in the region of high polymer contents caused by the high viscosity of the reactive mixture, the inadequate dissolution of the polymer, the poor mixing of the added nonsolvent, and the appearance of local turbidity. Such limitations are avoided based on the fact that polymer chains are produced homogenously in the bulk of a monomer/nonsolvent solution, and they precipitate thereafter. A schematic representation of the reaction path is shown in Figure 1. Since *n*-hexane is not consumed during the polymerization, the reaction path is represented by a simple straight line. Initially, the monomer/*n*-hexane mixture is a single homogeneous phase (point A in Fig. 1). The reaction proceeds homogeneously until the amount of PMMA in the system is high enough to induce the system phase separation (point B in Fig. 1). At that point, the mixture turns turbid and such turbidity can be detected to construct the ternary phase diagram. To determine the onset of turbidity, two techniques were applied: (1) visual examination; and (2) LLS. In what

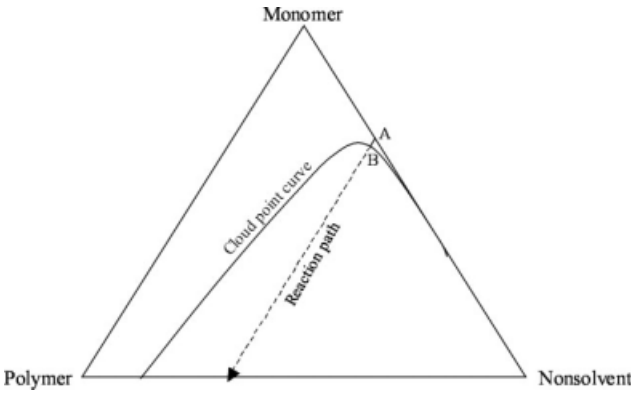

Figure 1 Schematic representation of an *in situ* polymerization on the ternary phase diagram: A, initial "homogeneous" solution of monomer/nonsolvent; B, polymerization cloud point.

follows, a description of the proposed techniques is provided.

Onset of turbidity by visual examination of polymerizing mixtures

Solutions of MMA/*n*-hexane/LPO of varying compositions were prepared, as shown in Table I (samples V1-V6). First, a LPO/MMA solution was prepared at room temperature and loaded into 4-mL glass vials. The initial concentration of LPO was 0.07 mol/L-MMA. Different amounts of *n*-hexane were added into the mixtures, and the vials were sealed and immersed in a clear water bath at 70°C to start the polymerization. The reaction mixtures in the vials reached the bath temperature in less than 3 min. The vials were taken from the bath as soon as their contents turned visually turbid. To stop the reaction after the contents became turbid, the vials were quenched in a cold ice-water bath, and hydroquinone inhibitor was added. Since the vial content was quite small, the temperature of the mixture was reduced very fast, and the amount of polymer produced during the quenching period was negligible. Also, hydroquinone dissolved easily in the polymer solution sample because of the relatively low monomer conversion reached at the cloud points. The amount of PMMA at the cloud point was determined by a standard gravimetric technique that consists of precipitating the polymer with methanol, filtering, and drying under vacuum until constant weight. Since the vials were sealed, it was assumed that the mass of *n*-hexane remained constant during the polymerization experiments. Table I illustrates the measured compositions for the investigated mixtures at the cloud points. Also presented in Table I are the reaction time required to reach the cloud point and the corresponding monomer conversion, calculated as the ratio between the mass of PMMA at the moment of phase separation and the initial mass of MMA.

At high *n*-hexane contents, the transition from a clear solution to a turbid solution occurred very fast, and the visual examination of the polymerizing monomer/*n*-hexane mixtures was quite accurate and reproducible. However, when using low nonsolvent contents, a significant amount of polymer was produced before reaching the cloud point (see Fig. 1), and the technique reproducibility was very poor. Specifically, the reaction mixtures in the vials exhibited partial turbidity because of high viscosity and hence, it was difficult to pinpoint the exact cloud point. For that reason, the results of recipes containing initial weight fraction of *n*-hexane lower than 0.379 are not reported in Table I.

Onset of turbidity by LLS technique

To improve the accuracy in determining the cloud points along the *in situ* polymerizations, and to

TABLE I
Initial Compositions and Compositions (weight Fractions) at the Cloud Points of MMA/*n*-Hexane Polymerizations with Visual Detection (V1-V6) and Online Laser Light Scattering Technique (LS1–LS8)

	Initial composition			Final composition at the cloud point				
Blend	*n*-hexane (—)	MMA (—)	PMMA (—)	*n*-hexane (—)	MMA (—)	PMMA (—)	Conversion (—)	Time (min)
V1	0.379	0.621	–	0.379	0.601	0.020	0.033	5.4
V2	0.443	0.557	–	0.443	0.540	0.017	0.031	8.3
V3	0.511	0.489	–	0.511	0.473	0.016	0.032	10.3
V4	0.582	0.418	–	0.582	0.405	0.013	0.031	13.4
V5	0.657	0.343	–	0.657	0.332	0.011	0.032	20.5
V6	0.819	0.181	–	0.819	0.175	0.006	0.032	36.3
LS1	0.098	0.902	–	0.098	0.271	0.630	0.699	28.0
LS2	0.151	0.849	–	0.151	0.209	0.640	0.753	33.7
LS3	0.207	0.793	–	0.207	0.448	0.345	0.435	35.3
LS4	0.233	0.767	–	0.233	0.583	0.184	0.240	32.8
LS5	0.375	0.625	–	0.375	0.608	0.017	0.027	11.8
LS6	0.514	0.486	–	0.514	0.472	0.014	0.029	8.6
LS7	0.651	0.349	–	0.651	0.338	0.011	0.032	12.9
LS8	0.819	0.181	–	0.819	0.176	0.005	0.028	17.9

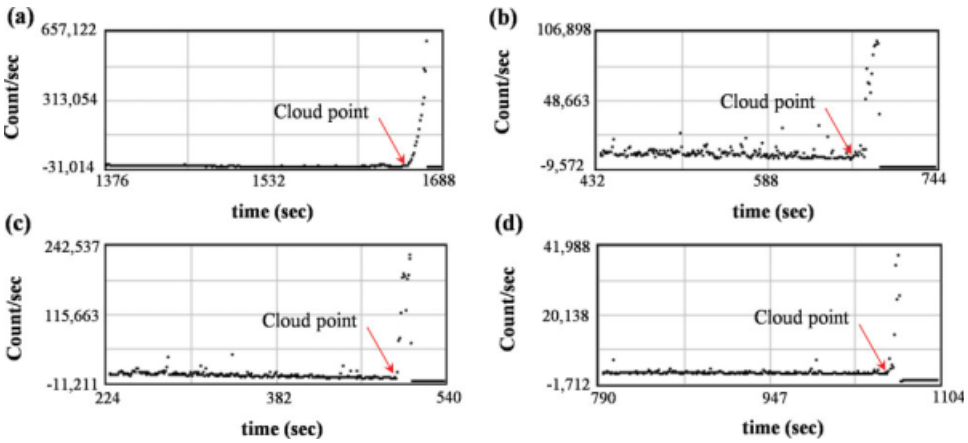

Figure 2 Number of photons scattered per second at an angle of 90° (arbitrary units) vs. polymerization time: (a) LS1, (b) LS5, (c) LS6, and (d) LS8. [Color figure can be viewed in the online issue, which is available at www.interscience.wiley.com.]

overcome the experimental difficulties of the visual examination technique in the region of high polymer contents, LLS was used to detect the nascent polymer precipitation. To this purpose, several MMA/*n*-hexane/LPO mixtures of known compositions were prepared in LLS cells (samples LS1-LS8 in Table I). The initial concentration of LPO was 0.07 mol/L-MMA. Cells were placed in the sample holder of a Photocor-FC light scattering instrument (Photocor) equipped with a 5 mW laser light source (JDS Uniphase, He-Ne laser, laser wavelength = 632.8 nm). The temperature was controlled by circulating water at 70°C through the sample holder jacket. The intensity of the scattered light at 90° was recorded during the polymerization. At the cloud point, an abrupt increase in the scattered light intensity was observed (see Fig. 2). Note that ordinates of Figure 2 exhibit arbitrary units because actual values are not required to detect the onset of polymer precipitation. After detecting the onset of turbidity, samples were quickly taken from the holder. LLS cells were immersed in a cold ice-water bath, after adding hydroquinone as inhibitor.

The compositions of the final mixtures shown in Table I were gravimetrically determined as explained in "Onset of Turbidity by Visual Examination of Polymerizing Mixtures" section. However, when the amount of polymer produced at the cloud point was too high (i.e., samples LS1-LS3), it was necessary to first dissolve the polymer in acetone before precipitating it with methanol. Note that the content of polymer at the cloud points of samples LS1 and LS2 are over 60%. As far as the authors are aware, this region of the ternary diagram has not been investigated before for solvent/nonsolvent/polymer systems due to the limitations of the conventional nonreactive titration technique.

Based on the determined cloud points for the samples of different compositions, a ternary phase diagram has been constructed (Fig. 3), and the following can be observed: (a) cloud points determined by visual examination of mixtures containing weight fractions of *n*-hexane between 0.379 and 0.819 are almost overlapped with the results obtained by LLS technique. This is a good indication of the accuracy of visual examination for determining cloud points in the region of relatively low polymer content; (b) as mentioned before, for *n*-hexane contents below 0.379, the reproducibility of visual examination technique was very poor and only LLS technique could be applied.

Some of the polymer samples taken at the system cloud points were analyzed to determine their molecular weights by gel permeation chromatography (GPC), using a UV detector and PLgel 10 μm MIXED-B columns (Polymer Laboratories). Chloroform was the mobile phase and PMMA standards of narrow molecular weight distribution were used to calibrate the column. Resulting average molecular weights are presented in Figure 4. It can be seen that molecular weights of the polymer produced in the LLS cells do not vary too much when comparing different samples. For instance, samples LS1-LS4 exhibit number-average molecular weights between 30,000 and 55,000 g/mol, and polydispersities in the order of 1.7 (Fig. 4). The effect of the polymer structure on the constructed phase diagram will be discussed in the next section.

Effect of the polymer molecular structure on the ternary phase diagram

Cloud points can be adopted as binodal points only when the polymer exhibits a very narrow molecular

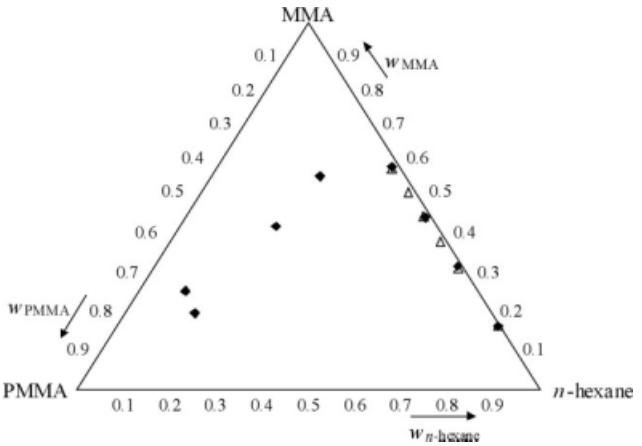

Figure 3 Cloud points measured along the polymerization of MMA in the presence of *n*-hexane at 70°C. (△) Visual examination; (■) light scattering method.

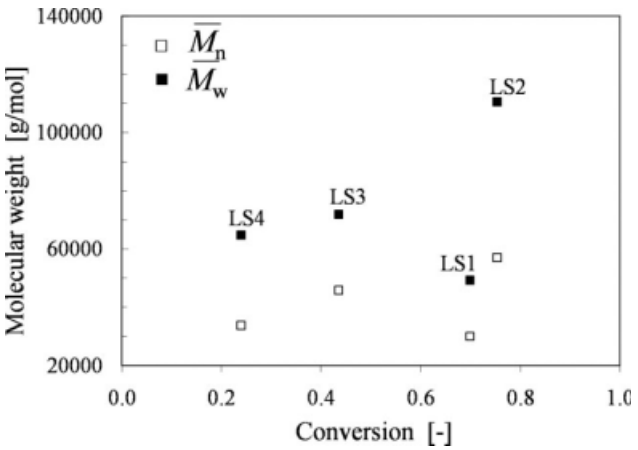

Figure 4 Average molecular weights of PMMAs produced in LLS cells at the cloud points.

weight distribution.[6] However, PMMAs produced via industrial free radical polymerizations are mostly polydisperse, exhibiting broad molecular weight distributions. The PMMAs produced in this work by the proposed *in situ* free radical polymerization also show a relatively high polydispersity, and its effect on the cloud points needs to be tested. For that reason, the compositions of the cloud points for several MMA/PMMA/*n*-hexane mixtures containing PMMAs of different molecular structures were determined at 70°C. As mentioned before, *in situ* polymerizations cannot be used to produce monodisperse PMMA. Instead, the experiments were carried out by simple titration of the MMA/PMMA mixtures with *n*-hexane, using PMMAs of known molecular structures. Unfortunately, only the region of low polymer content could be investigated by this technique.

Four PMMA samples of known molecular weights were studied (see Table II). $PMMA_1$ and $PMMA_2$ were GPC standards of low polydispersity, while $PMMA_3$ and PMM_4 were synthesized in our labs by dispersion polymerization of MMA in the presence of *n*-hexane at 70°C for 1.5 h. More details of the synthesis procedure can be found in the next section. As shown in Table II, this heterogeneous precipitation polymerization produces materials of quite high polydispersity. To determine the cloud points, known amounts of the investigated PMMAs were mixed together with MMA in sealed vials at room temperature until a complete dissolution of polymers was observed. For each PMMA sample, two PMMA/MMA initial ratios were tested (i.e., ~ 0.015 and 0.03 in weight). Vials were immersed in a water bath at 70°C for 1 h, and small aliquots of *n*-hexane were added with a micropipette. Compositions at the system cloud points were determined by measuring the mass of nonsolvent required to induce a slight turbidity to the mixtures.

Experimental results are presented in Table II. As expected, the polymer molecular characteristics do not affect significantly the composition of the cloud points.[16–20] However, the effect could be more important for polymers of low molecular weights. Another important observation from the results in Table II is that a wider heterogeneous region is

TABLE II
Effect of the Polymer Molecular Structure on the Cloud Points of MMA/PMMA/*n*-Hexane System at 70°C

Polymer characteristics			Initial composition	Compositions at the cloud point		
Sample	$\overline{M}_n$ (g/mol)	$\overline{M}_w/\overline{M}_n$ [−]	PMMA/MMA ratio (wt)	MMA	*n*-Hexane	PMMA
$PMMA_1$[a]	30,454	1.10	0.025	0.857	0.121	0.022
			0.013	0.863	0.126	0.011
$PMMA_2$[a]	119,811	1.06	0.031	0.856	0.117	0.027
			0.016	0.903	0.082	0.015
$PMMA_3$[b]	114,000	3.36	0.025	0.868	0.110	0.022
			0.011	0.888	0.101	0.011
$PMMA_4$[b]	137,200	4.51	0.029	0.850	0.125	0.025
			0.016	0.890	0.095	0.015

[a] Characterized by provider.
[b] Characterized by GPC in our labs.

measured when applying the titration method (with respect to the results shown in Fig. 3). In part, this is caused by the limited dissolution of the added nonsolvent into the mixture that promotes the appearance of local turbidity even when the mixture is still homogeneous. Due to the limitation of the titration technique, only cloud points of lower polymer content were investigated.

Conversion curve along a dispersion polymerization of MMA in *n*-hexane

To investigate the behavior of the polymerization system at higher conversions, a dispersion polymerization was carried out until complete depletion of the monomer. To this purpose, several mixtures were prepared containing the same initial compositions as LS4 (Table I). To this purpose, monomer and LPO were mixed together in 4 mL vials, and a solution of *n*-hexane containing 0.0027 mol/L-MMA of PDMS was added into the mixtures. Vials were sealed and immersed in the water bath at 70°C. At prespecified reaction times, they were taken from the bath, and hydroquinone was added to stop the polymerization.

For each sample, the monomer conversion was gravimetrically determined, and the results are presented in Figure 5. The conversion curve shows the typical S-shape produced by an early gel effect. The process auto-acceleration is observed at monomer conversions close to the system phase separation point. This is due to the appearance of the second (polymer-rich) phase. In this phase, the mobility of the growing macro-radicals is highly limited even at low conversion, thus promoting an early and strong gel effect.

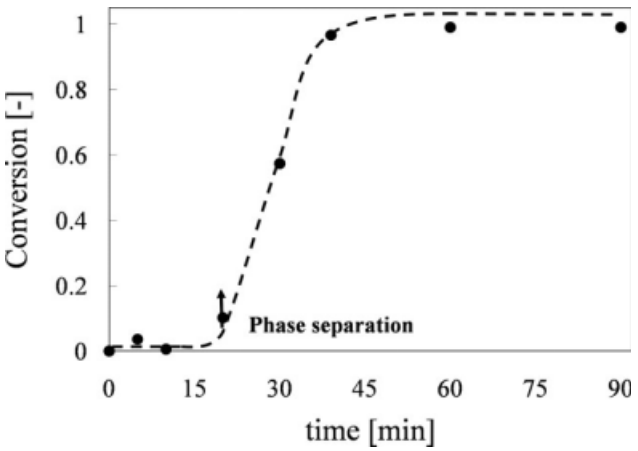

Figure 5 Evolution of the monomer conversion for the dispersion polymerizations of MMA in *n*-hexane at 70°C (initial weight fraction of *n*-hexane = 0.23). Arrow indicates the moment where the system phase separation took place (Table I). Dashed trace is added to guide the eye only.

THEORETICAL WORK

Construction of the theoretical ternary phase diagram

A mathematical model capable of predicting the ternary phase diagram for a three-component system is an important tool for the design and control of heterogeneous polymerization process where phase separation occurs during the course of the polymerization. The binodal and spinodal curves subdivide the ternary diagram into stable, metastable, and unstable regions. While the binodal curve delimits the stable from the metastable regions, the spinodal curve delimits the metastable from the unstable regions. Different morphological structures can be produced according to the region in which the phase separation occurs.

In this work, we shall use the well-known FH theory of polymer solutions[21] to construct a theoretical ternary phase diagram for the MMA/PMMA/*n*-hexane system. For a ternary system at equilibrium, the Gibbs free energy of mixing (ΔG_m) can be expressed as follows:

$$\frac{\Delta G_m}{RT} = \sum_{i=\mathrm{M,P,S}} n_i \ln(\phi_i) + \chi_{\mathrm{S,P}} n_\mathrm{S} \phi_\mathrm{P} + \chi_{\mathrm{M,P}} n_\mathrm{M} \phi_\mathrm{P} + \chi_{\mathrm{S,M}} n_\mathrm{S} \phi_\mathrm{M} \quad (1)$$

where n_i and ϕ_i are the number of moles and the volume fractions of species (with i = M (monomer), P (polymer), S (nonsolvent) indicating MMA, PMMA, and *n*-hexane, respectively), $\chi_{i,j}$ is the interaction parameter between species i and j, R is the gas constant, and T is the absolute temperature. Based on the results in "Effect of the Polymer Molecular Structure on the Ternary Phase Diagram" section, the effect of polymer molecular weight on the ternary phase diagram was neglected. Therefore, cloud points and binodal points were assumed to be the same. Also, it was assumed that $\chi_{i,j}$ is independent from the phase composition. This simplification is somewhat crude, because in many cases a strong dependence between the interaction parameters and the composition of the phases can be observed. However, to take into consideration of such dependence, it is necessary to include new adjustable parameters that may also bring new uncertainties. Also, measurements of the system tie lines should be required. This is outside the scope of this article that simply uses the theoretical predictions of the ternary diagram as a tool to interpret the behavior of precipitation and/or dispersion polymerizations.

From eq. (1), the chemical potential for each species referred to the standard state ($\Delta\mu_{i,k}$) can be written as follows[6]:

$$\frac{\Delta\mu_{S,k}}{RT} = \ln(\phi_{S,k}) + 1 - \phi_{S,k} - s\phi_{M,k} - r\phi_{P,k} + (\chi_{S,M}\phi_{M,k} + \chi_{S,P}\phi_{P,k})(\phi_{M,k} + \phi_{P,k}) - s\chi_{M,P}\phi_{M,k}\phi_{P,k} \quad (2)$$

$$s\frac{\Delta\mu_{M,k}}{RT} = s\ln(\phi_{M,k}) + s - \phi_{S,k} - s\phi_{M,k} - r\phi_{P,k} + (\chi_{S,M}\phi_{S,k} + s\chi_{M,P}\phi_{P,k})(\phi_{S,k} + \phi_{P,k}) - \chi_{S,P}\phi_{S,k}\phi_{P,k} \quad (3)$$

$$r\frac{\Delta\mu_{P,k}}{RT} = r\ln(\phi_{P,k}) + r - \phi_{S,k} - s\phi_{M,k} - r\phi_{P,k} + (\chi_{S,P}\phi_{S,k} + s\chi_{M,P}\phi_{M,k})(\phi_{S,k} + \phi_{M,k}) - \chi_{S,M}\phi_{S,k}\phi_{M,j} \quad (4)$$

where subscript k indicates the phase (1 = nonsolvent-rich phase, 2 = polymer-rich phase); s and r are the molar volume ratios of nonsolvent/monomer and nonsolvent/polymer, respectively. To calculate the molar volume of the polymer, the number-average molecular weight ($\overline{M}_n$) was used.

For a given total composition of the mixture, the partition coefficients can be defined as the ratio between the concentration of a species in the polymer-rich phase and that in the nonsolvent-rich phase, as follows:

$$K_i = \frac{\phi_{i,2}}{\phi_{i,1}} \quad i = \mathrm{M,P,S} \quad (5)$$

The binodal points are determined by calculating the composition of the phases that produce equal chemical potentials of the species in both phases (i.e., $\Delta\mu_{S,1} = \Delta\mu_{S,2}$, $\Delta\mu_{M,1} = \Delta\mu_{M,2}$, and $\Delta\mu_{P,1} = \Delta\mu_{P,2}$). Tie lines can be constructed by connecting the compositions of mutually stable binodal points. In this work, binodal points were estimated through a well-known iterative procedure that adopts the volume fraction of MMA in the polymer-rich phase ($\varphi_{M,2}$) as the independent variable.[6,22] First, the volume fraction of PMMA in the *n*-hexane-rich phase is set to zero ($\varphi_{P,1} = 0$). Then, the following iterative cycle is applied to determine the five unknown variables (i.e., $\varphi_{S,1}$, $\varphi_{S,2}$, $\varphi_{M,1}$, $\varphi_{P,2}$ and the actual value of $\varphi_{P,1}$)[6]:

i. The volume fractions of nonsolvent in both phases ($\phi_{S,1}$, $\phi_{S,2}$) are obtained by minimizing the quadratic objective function $F = (\Delta\mu_{S,1} - \Delta\mu_{S,2})^2 + (\Delta\mu_{M,1} - \Delta\mu_{M,2})^2$.
ii. A new value of the volume fraction of polymer in the nonsolvent-rich phase ($\phi_{P,1}^{new}$) is calculated by solving the nonlinear equation $\Delta\mu_{P,1} - \Delta\mu_{P,2} = 0$.
iii. After setting $\phi_{P,1} = \phi_{P,1}^{new}$, the iterative cycle is restarted in (i) until $|\phi_{P,1} - \phi_{P,1}^{new}| \rightarrow 0$.

To analyze the metastable region of heterogeneous processes, it is also important to calculate the spinodal curve. Critical points in multicomponent systems can be estimated by the method of Gibbs determinants. In our ternary system, the spinodal is determined from the following condition for the monomer and polymer[23,24]:

$$\begin{vmatrix} G_{M,M} & G_{M,P} \\ G_{P,M} & G_{P,P} \end{vmatrix} = 0 \quad (6)$$

$G_{i,j}$ is defined as $\left.\frac{\partial^2 \overline{\Delta G_m}}{\partial\phi_i\partial\phi_j}\right|_{P,T}$ where $\overline{\Delta G}_m$ is the dimensionless unit-volume based Gibbs free energy of mixing. Using eqs. (1) and (6), and the definition of $G_{i,j}$, the following condition can be obtained for the spinodal curve of a monomer/polymer/nonsolvent ternary system[22–24]:

$$G_{M,M}G_{P,P} - (G_{M,P})^2 = 0 \quad (7)$$

with:

$$G_{M,M} = \frac{1}{\phi_S^*} + \frac{s}{\phi_M^*} - 2\chi_{S,M} \quad (8)$$

$$G_{P,P} = \frac{1}{\phi_S^*} + \frac{r}{\phi_P^*} - 2\chi_{S,P} \quad (9)$$

$$G_{M,P} = \frac{1}{\phi_S^*} - (\chi_{S,M} + \chi_{S,P}) + s\chi_{M,P} \quad (10)$$

where ϕ_M^*, ϕ_P^*, and ϕ_S^* are the volume fractions of monomer, polymer, and nonsolvent corresponding to spinodal conditions. To solve eq. (7), ϕ_P^* was adopted as the independent variable, and the corresponding ϕ_S^* was obtained by calculating the roots of the following equation:

$$[1/\phi_S^* + s/(1 - \phi_S^* - \phi_P^*) - 2\chi_{S,M}][1/\phi_S^* + r/\phi_P^* - 2\chi_{S,P}] - [1/\phi_S^* - (\chi_{S,M} + \chi_{S,P}) + s\chi_{M,P}]^2 = 0 \quad (11)$$

Model adjustment and simulation results

To match the model simulation results with the experimental ternary composition data, it was assumed that the presence of a chemical initiator has negligible effect on the phase equilibrium because its initial concentration is very low (less than 0.1 wt % of the initial amount of monomer) and it decreases with reaction time. The model parameters used in our calculations are presented in Table III. Except for χ_{SM}, all the other parameters were directly taken from

TABLE III
Model Parameters

Parameter	Value	Reference
Interaction parameters		
χ_{SP} (—)	1.623	3,25
χ_{MP} (—)	0.412	25,26
χ_{SM} (—)	1.850	This work
Physical constants		
ρ_M (g L^{-1})	886.8	27
ρ_S (g L^{-1})	613.4	28
ρ_P (g L^{-1})	1153.0	29

the literature. The value of χ_{SM} was adjusted to minimize the maximum difference between simulated and experimental results. Because of its improved accuracy, only the results from LLS were used for the model adjustment.

Figure 6 presents the model-predicted binodal and spinodal curves together with the tie lines. Also shown are the experimental data measured by LLS technique. For these simulations, the number-average molecular weight of the PMMA was adopted as 50,000 g/mol. The following can be observed in Figure 6: (a) predicted binodal curve (solid line) fits reasonably well the experimental results from LLS technique, (b) except for the upper region of the ternary diagram where partial miscibility between *n*-hexane/MMA and polymer is observed, the nonsolvent-rich phase exhibit a negligible amount of dissolved polymer; and (c) binodal points corresponding to the nonsolvent-rich phase are almost overlapped with spinodal points, but this is not the case for the region close to the polymer-rich phase (where binodal and spinodal curves are quite separated one from each other). At the right hand side of the ternary diagram, spinodal decomposition mechanism governs the phase separation process, while at the left hand side, the controlling mechanism is nucleation and growth.[30]

We now consider the species partition coefficients predicted by the model for fixed fractions of nonsolvent (Fig. 7). Note that abscissas correspond to the ratio between the mass fraction of polymer and the mass fraction of polymer + monomer. This variable is analogous to the monomer conversion along a polymerization path. The following can be observed in Figure 7: (i) at high *n*-hexane contents (w_S), the phase separation occurs at values of abscissas close to zero. When the *n*-hexane content is lower (e.g., $w_S = 0.2$), however, the phase separation occurs at $w_P/(w_M + w_P) = 0.215$. At monomer conversions $x < 0.215$, the system exhibits a single phase and calculation of species partition coefficients has no physical sense; (ii) at relatively high *n*-hexane contents, monomer accumulates preferentially in the polymer-rich phase, thus resulting $K_M > 1$ [Fig. 7(a)]; (iii) except for a small region of partial miscibility at $w_S = 0.2$ [see insert in Fig. 7(b)], the polymer concentration in the polymer-rich phase is as much as 13 order of magnitude higher than that in the nonsolvent-rich phase, suggesting that the *n*-hexane-rich phase contains practically no polymers [Fig. 7(b)]; (iv) as expected, *n*-hexane accumulates preferentially in the nonsolvent-rich phase due to its thermodynamic incompatibility with the polymer, thus resulting $K_S < 1$ [Fig. 7(c)]. Perhaps, the most important implication of observation (iii) is that as soon as polymer is formed in the nonsolvent-rich phase, it has to migrate to the polymer-rich phase to reach the thermodynamic equilibrium. In a real

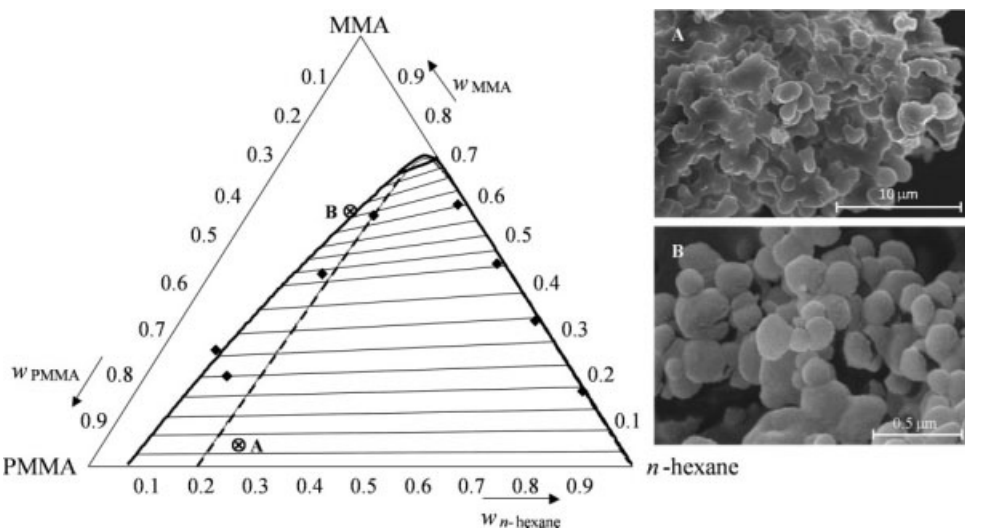

Figure 6 Theoretical ternary diagram and experimental data: (—) Binodal curve (calculations); (— —) spinodal curve (calculations); (—) tie lines (calculations); (◆) cloud points experimentally measured by LLS technique. For samples collected at points A and B on the ternary diagram, the SEM pictures are also presented (see right-hand side).

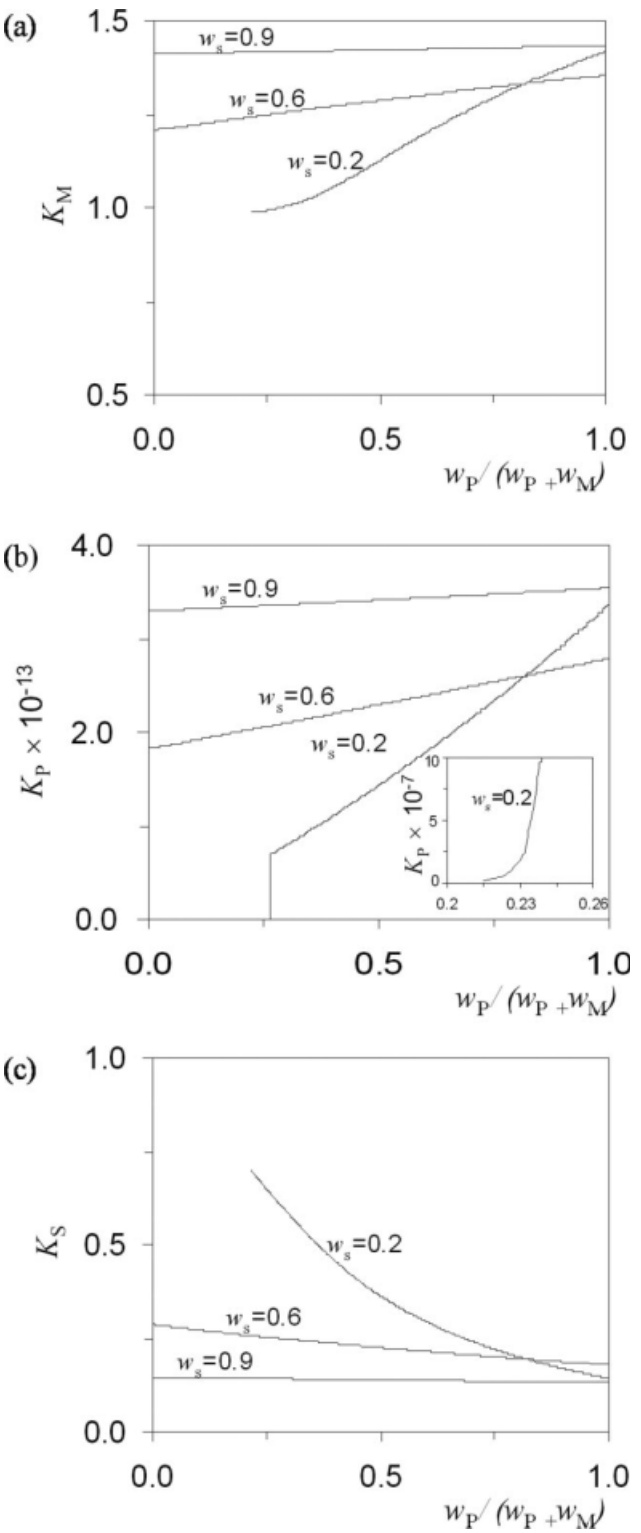

Figure 7 Evolution of species partition coefficients for different fractions of nonsolvent (w_S). (a) monomer; (b) polymer; (c) nonsolvent.

polymerization process, however, thermodynamic equilibrium may not be reached instantaneously due to both the low diffusivity of the produced polymer chains and the relatively low reaction times. This effect should be more pronounced at higher conversions.

Recall that, for simulation purposes, the number-average molecular weight of the polymer was set to 50,000 g/mol. In Figure 8, the predicted effect of the polymer molar weight on the binodal and spinodal curves is shown. Except for a small region close to the system critical point, calculated binodal and spinodal curves are not affected significantly.

Finally, let us consider the predicted ternary phase diagram in Figure 6 and its potential effects on a precipitation and/or dispersion polymerization of MMA in the presence of *n*-hexane. First of all, the ternary diagram is helpful to understand the effect of phase separation on the molecular structure of the generated polymer. After the phase separation point, a stronger gel effect affects the viscous polymer-rich phase, while in the (polymer-free) nonsolvent-rich phase diffusion controlled reactions should be negligible. Polymer chains with relatively high molecular weights will be generated in the polymer-rich phase, and polymer chains with lower molecular weights will be generated in the nonsolvent-rich phase. As a result, quite wide or even bimodal molecular weight distributions are expected to be produced after phase separation point. This observation has been confirmed experimentally (see molecular characteristics of polydisperse polymers $PMMA_3$ and $PMMA_4$ in Table II).

As explained before, the reaction paths of a precipitation polymerization can be represented by straight lines parallel to the MMA/PMMA axis. According to Figure 6, reactions carried out with very low solvent contents (below 7%) will proceeds in a single phase from the beginning to the end of the polymerization. Therefore, material's final morphology produced via reactions in a single phase should be similar to those obtained by a simple bulk

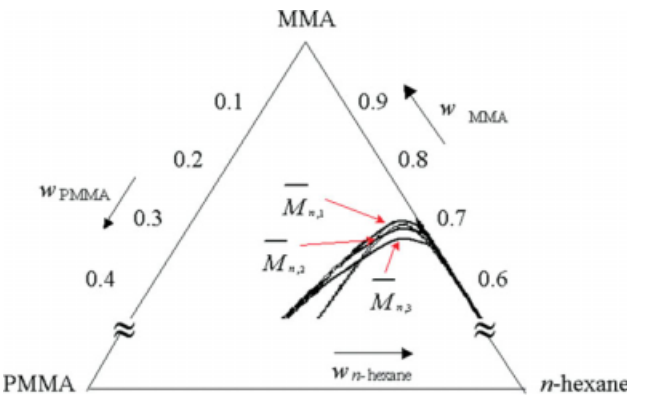

Figure 8 Effect of the number-average molecular weight of PMMA on the binodal (—) and spinodal (--) curves. $\overline{M}_{n,1}$ = 100,000 g/mol; $\overline{M}_{n,2}$ = 50,000 g/mol; and $\overline{M}_{n,3}$ = 25,000 g/mol. [Color figure can be viewe din the online issue, which is available at www.interscience.wiley.com.]

polymerization of MMA. For contents of *n*-hexane between 7% and 20%, the polymerization exhibits an initial homogeneous stage, followed by a heterogeneous stage (after the reaction path intersects the binodal curve). Immediately after the system phase separation, the polymerization mixture enters a metastable region where nucleation and growth mechanism will govern the morphology development.[30] For initial contents of *n*-hexane over 20%, the phase separation occurs almost immediately after the polymerization start. In this case, spinodal decomposition mechanism should control the phase separation.[30] For instance, Figure 6 shows the SEM images for polymer samples taken at different reaction extents of dispersion polymerizations of MMA. Reactions were carried out using initial weight fractions of *n*-hexane of 0.15 and 0.23, and the same experimental procedure and recipes as indicated in "Conversion Curve Along a Dispersion Polymerization of MMA in *n*-Hexane" section. To stabilize the precipitating polymer particles, PDMS was added into the reaction mixtures, and they were agitated with a magnetic stirrer at 500 rpm. SEM images show a pronounced difference in the particle size (see right hand side of Fig. 6). Using an initial weight fraction of *n*-hexane of 0.15, the particle size is big at relatively low monomer conversions (diameters of 2 μm at $x\sim$ 30%). In contrast, using an initial weight fraction of *n*-hexane of 0.23, particles diameter is much smaller even when the monomer has been almost completely consumed (diameter less than 0.5 μm at $x\sim$ 90%). These observations illustrate that understanding the characteristics of the reaction path along the ternary phase diagram would be important to control the polymer particle morphology in dispersion polymerization processes.

CONCLUSIONS

In this article, the *in situ* polymerization of MMA in the presence of a nonpolar nonsolvent such as *n*-hexane was investigated with the final aim of constructing the complete ternary phase diagram for the MMA/PMMA/*n*-hexane system. In situ polymerization with online LLS detection technique has been found to be very effective to determine the composition of cloud points in the region of high polymer contents where conventional titration technique fails. The theoretical model derived from the FH theory has also been used to calculate the binodal and spinodal points. Both experimental determinations and theoretical results were used to elucidate possible implications on the precipitation polymerization of MMA in the presence of *n*-hexane. The results of this article will be used in future works to investigate the macro- and microdispersion polymerization of MMA in the presence of a nonpolar hydrocarbon solvent.

NOMENCLATURE

K_i Partition coefficient of species i [-]
n_i Number of moles of species i [mol]
R Gas constant [cal/(mol K)]
T Absolute temperature [K]
w_i Weight fraction of species i [-]

GREEK SYMBOLS

ΔG_m Gibbs free energy of mixing [cal]
$\Delta\mu_i$ Chemical potential of specie i referred to the standard state [cal/mol]
ρ_i Mass density of species i [g/L]
$\phi_{i,k}$ Volume fraction of species i in phase k [-]
$\chi_{i,j}$ Interaction parameter between species i and j [-]
s Solvent/monomer molar volume ratio [-]
r Solvent/polymer molar volume ratio [-]

SUBSCRIPTS

i,j Species (M = monomer, P = polymer, S = solvent)
k Phase (1 = solvent-rich phase, 2 = polymer-rich phase)

SUPERSCRIPTS

* Condition at the spinodal curve

The authors thank the assistance of Hee Young Lee in LLS experiments and the help of Laleh Emdadi in the precipitation polymerizations.

References

1. Meira, G. R.; Luciani, C. V.; Estenoz, D. A. Macromol React Eng 2007, 1, 25.
2. Alexopoulos, A. H.; Kiparissides, C. Chem Eng Sci 2007, 62, 3970.
3. Dong, R.; Zhao, J.; Zhang, Y.; Pan, D. J Polym Sci Part B: Polym Phys 2009, 47, 261.
4. Cohen, C.; Tanny, G. B.; Prager, S. J Polym Sci Polym Phys Ed 1979, 17, 477.
5. Soh, Y. S.; Kim, J. H.; Gryte, C. C. Polymer 1995, 36, 3711.
6. Lai, J. Y.; Lin, S. F.; Lin, F. C.; Wang, D. M. J Polym Sci Part B: Polym Phys 1998, 36, 607.
7. Young, T. H.; Cheng, L. P.; Hsieh, C. C.; Chen, L. W. Macromolecules 1998, 31, 1229.
8. Wang, D.; Li, K.; Teo, W. K. J Appl Polym Sci 1999, 71, 1789.
9. Lin, K. Y.; Wang, D. M.; Lai, J. Y. Macromolecules 2002, 35, 6697.
10. Wang, B.; Dar, Y.; Shi, L.; Caneba, G. T. J Appl Polym Sci 1999, 71, 761.
11. Tao, C. T.; Young, T. H. Polymer 2005, 46, 10077.
12. Barzin, J.; Sadatnia, B. Polymer 2007, 48, 1620.
13. Young, T. H.; Tao, C. T.; Lai, P. S. Polymer 2003, 44, 1689.
14. Cheng, L. P.; Shaw, H. Y. J Polym Sci Part B: Polym Phys Ed 2000, 38, 747.

15. Aggarwal, A.; Saxena, R.; Wang, B.; Caneba, G. T. J Appl Polym Sci 1996, 62, 2039.
16. Baysal, B.; Stockmayer, W. J. Polym Sci 1967, 5, 315.
17. Kamide, K.; Matsuda, S.; Miyazaki, Y. Polym J 1984, 16, 479.
18. Kamide, K.; Matsuda, S. Polym J 1984, 16, 515.
19. Kamide, K.; Matsuda, S. Polym J 1984, 16, 591.
20. Kamide, K.; Matsuda, S. Polym J 1985, 18, 347.
21. Flory, P. Principles of Polymer Chemistry; Cornell University Press: Ithaca, 1953.
22. Yilmaz, L.; Mchugh, A. J. J Appl Polym Sci 1986, 31, 997.
23. Tompa, H. Polymer Solutions; Butterworths Scientific Publications: London, 1956.
24. Šolc, K.; Koningsveld, R. J Phys Chem 1985, 89, 2237.
25. Hughes, L. J.; Britt, G. E. J Appl Polym Sci 1961, 5, 337.
26. Brandrup, J.; Immergut, E. Polymer Handbook, 3rd ed.; Wiley: New York, 1989.
27. Steele, W.; Chirico, R.; Cowell, A.; Knipmeyer, S.; Nguyen, A. J Chem Eng Data 2002, 47, 700.
28. Lide, D. CRC Handbook of Chemistry and Physics, 84th ed.; CRC Press: New York, 2004.
29. Tefera, N.; Weickert, G.; Westerterp, K. R. J Appl Polym Sci 1997, 63, 1663.
30. Saxena, R.; Caneba, G. T. Polym Eng Sci 2002, 42, 1019.